Research Article | Vol. 33, No. 17 / 25 Aug 2025 / Optics Express 36208

Optics EXPRESS

270 km single-span distributed fiber-optic vibration sensor without optical amplification

GEORGE Y. CHEN,[1,2] SHANGWEI DAI,[1,2] XING RAO,[1,2] HANJIE LIU,[1,2] AND YIPING WANG[1,2,*]

[1]Key Laboratory of Optoelectronic Devices and Systems of Ministry of Education and Guangdong Province, College of Physics and Optoelectronic Engineering, Shenzhen University, Shenzhen 518060, China
[2]Shenzhen Key Laboratory of Photonic Devices and Sensing Systems for Internet of Things, Guangdong and Hong Kong Joint Research Centre for Optical Fiber Sensors, Shenzhen University, Shenzhen 518060, China
[*]ypwang@szu.edu.cn

Abstract: With our ever-expanding cities and interconnected cities, smart monitoring for long-distance railway tracks and natural hazards is imperative. Conventional distributed acoustic sensors (DAS) rely on backscattered signals along the optical fiber, which limit their maximum sensing distance and signal-to-noise ratio. Long-distance forward transmission distributed sensing systems typically use a double-ended detection strategy with bidirectional optical propagation, and the maximum sensing distance is constrained by backscatter noise rather than optical power. Rayleigh backscattering (RBS) and coherent noise arising from backscattered light mix in with the forward transmitted signals, resulting in a reduced signal-to-noise ratio. To separate backscatter from forward transmission, an acousto-optic frequency-shifted forward transmission distributed vibration sensor (AFS-FTDVS) design is proposed, which can facilitate vibration sensing over long distances without the need for optical amplification. A positioning accuracy of 35.6 m was demonstrated along a 272 km-long single-mode fiber. In addition, a tensile test of submarine optical cable was carried out to simulate the monitoring of seabed events. The experimental results reveal that the sensing system can precisely measure and locate low-frequency (0.15 Hz) stretching events along a 180 km long submarine cable, which provides the groundwork for an ocean-spanning natural disaster observation network.

1. Introduction

In order to satisfy the requirements of long-distance distributed sensing, forward-transmission distributed vibration sensors (FTDVS) (or "forward DAS") have been proposed as a viable long-distance alternative to optical time-domain reflectometry (OTDR) schemes [1]. These sensing systems typically utilize the interference of light propagating in the forward direction (can be either direction) instead of backscattered light, resulting improved signal-to-noise ratio over long distances [2–4]. These features make them very suitable [5] for applications such as intrusion detection [6], structural monitoring [7,8], and perimeter security [9]. In 2007, Shan S et al. proposed to use a Dual Mach-Zehnder interferometer (DMZI) structure to realize oil pipeline leakage detection, and achieved a positioning error of 200 m within a sensing range of 50 km [10]. In 2014, S. Pi et al [11]. utilized a 100 km Sagnac interferometer (SI) to attain a positioning error within 50 m for simulated intrusion events. In 2021, Huang J et al proposed a hybrid configuration of dual-SI incorporating a polarization compensation module, and achieved a 150 km sensing distance with a positioning error of ±30 m [12]. In order to further improve the sensing distance, optical amplifiers are commonly used to offset optical loss. Q. Chen et al. introduced a FTDVS based on a unidirectional DMZI, which utilize chromatic dispersion between two wavelength channels to determine the vibration position. They achieved a sensing distance of 320 km using multi-stage EDFA amplification [13]. Kong W et al proposed an FTDVS system based on phase difference and endpoint amplification, which maintains a positioning accuracy

#567378 https://doi.org/10.1364/OE.567378
Journal © 2025 Received 8 May 2025; revised 1 Aug 2025; accepted 4 Aug 2025; published 15 Aug 2025

Optics EXPRESS

within ±51 m across frequencies from 300 Hz to 10 kHz over a 122 km range [14]. Yan Y et al built an ultra-long distributed vibration sensor using a frequency-shifted optical delay line consisting of an acousto-optic modulator and a time delay fiber which can realize a sensing distance of 1230 km [15]. Feng Shi et al proposed an interferometric distributed fiber-optic sensing system based on ultra-low-loss fiber with a sensing range over 300 km, which employs a Raman fiber amplifier with bidirectional pumping in conjunction with a bidirectional EDFA [16].

Previously, researchers used either muti-core fiber parallel transmission or unidirectional transmission [17] to avoid backscatter noise mixing with the transmitted light. However, this significantly increases the cost. Others researchers had proposed dual-wavelength transmission with DWDM (Dense Wavelength Division Multiplexer) to suppress the backscatter noise in bidirectional single-mode fiber-based sensing systems. For example, Ma C et al. demonstrated a single span of 60 km using an ADMZI (Asymmetric Dual Mach–Zehnder interferometry) structure [18]. Xing Rao et al reported a FTDVS system based on dual wavelength and self-interference, which can realize single-span sensing distances up to 150 km [19]. Furthermore, multi-wavelength designs require an additional laser source and demodulation hardware, which raises the cost. However, the phase signals between the two wavelength channels (directions) inherently suffers from distortion, which reduces the positioning accuracy when using algorithms such as cross-correlation [20].

In general, the maximum sensing distance of doubled-ended FTDVS is limited not by the optical power, but by backscatter noise. Although a single-direction system design mitigates this problem, it suffers from poorer positioning accuracy due to having to utilize the dispersion effect [13]. In order to suppress RBS noise and achieve long-distance vibration sensing, we propose an acousto-optic frequency-shifted forward transmission distributed vibration sensing (AFS-FTDVS) system design. The Rayleigh backscattering interference signal can be separated from the forward optical signal in the frequency domain by applying an acousto-optic modulator (AOM) to frequency shift certain optical propagation direction. At the receiver end, the signal and RBS noise possess different beat frequencies, which allows the RBS noise to be filtered out. The elegant use of a single modulator instead of specialty fiber or multiple wavelengths allows the system cost to be considerably reduced.

2. System configuration and analysis

The experimental setup of the AFS-FTDVS system is shown in Fig. 1(a). The system consists of two parts: the optical system and the sensing fiber loop. The optical system launches continuous-wave light into the sensing fiber loop, beat the output signal with reference light in the 90° optical hybrid to generate I/Q components, and convert the beat signal into radio frequency (RF) signals using the balanced photodetector (BPD). The sensing loop is the fiber under test, which is either standalone single-mode fiber (SMF) or SMF protected within a submarine cable (indoor environment).

The laser source used is NKT Koheras BASIK E15, which exhibits a linewidth of <100 Hz and low phase noise. The laser output is split into the clockwise (CW) beam and the counter-clockwise (CCW) beam by the optical coupler OC1. The CW beam passes through an AOM and experiences a frequency shift of Δf = 200 MHz to realize the heterodyne configuration. Then both CW beam CCW beams are divided into reference light E_{r1}, E_{r2} and sensing light E_{s1}, E_{s2} by OC2 and OC3 respectively. The sensing light is transmitted into the sensing loop through optical circulator (Cir) and mixes with the reference light in the 90° optical hybrid (Hybrid). Note that E_{s1} outputs from Cir 2 and interferes with E_{r1} in Hybrid 1, E_{s2} outputs from Cir 1 and interferes with E_{r2} in Hybrid 2. Due to the presence of two beams propagating in opposite directions in the sensing fiber, their backscattering E_{RBS1} and E_{RBS2} are in the same direction as the propagation direction of the opposing transmission beam. At the same time, after passing through the Cir, they interfere with the reference light in the hybrid, resulting in aliasing of the backscattered and

Optics EXPRESS

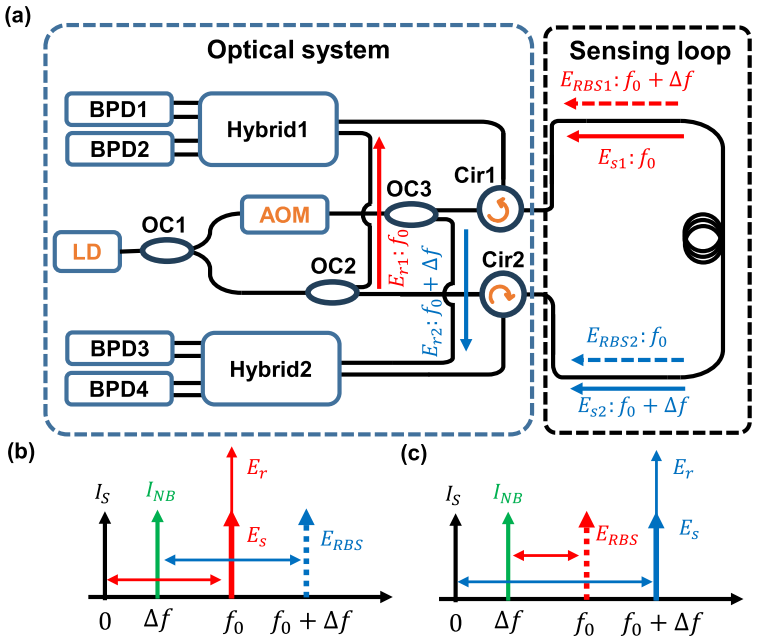

Fig. 1. Proposed AFS-FTDVS system and the frequency separation method for forward transmitted and backscattered light: (a) Schematic of system setup, OC: Optical couple, AOM: Acousto-optic Modulators, LD: Laser diode, BPD: Balanced photodetector, Hybrid: 90° optical hybrid, Cir: Optical circulator; (b) Interference-generated frequency components between signal light and reference light in Hybrid1; (c) Interference-generated frequency components between signal light and reference light in Hybrid2.

forward propagating probe light. Considering that the interference signal components approach zero beyond the coherent length of the laser, the interference signal output by the Hybrid 1 and Hybrid 2 can be expressed as:

$$\begin{cases} I_1(t) = I_{S1}(t) + I_{RBS1}(t) + I_{RBSS1}(t) \\ I_2(t) = I_{S2}(t) + I_{RBS2}(t) + I_{RBSS2}(t) \end{cases} \tag{1}$$

where I_{S1} represents the interference between E_{s1} and E_{r1}. The noise components include I_{RBS1} and I_{RBSS1}. The term I_{RBS1} comprises E_{r1} and E_{RBS1}, while I_{RBSS1} is formed from E_{s1} and E_{RBS1}. Neglecting laser phase noise, these three components can be expressed by the following equations:

$$\begin{aligned} I_{S1}(t) &= |E_{r1}(t) + E_{s1}(t)|^2 \\ &= |\varepsilon_{in} \exp(-j2\pi f_0 t) + \varepsilon_\tau \exp[-j(2\pi f_0 t + \varphi(t))]|^2 \\ &= \varepsilon^2{}_{in} + \varepsilon^2{}_{\tau} + 2\varepsilon_{in}\varepsilon_\tau \cos\varphi(t) \end{aligned} \tag{2}$$

$$\begin{aligned} I_{RBS1}(t) &= |E_{r1}(t) + E_{RBS1}(t)|^2 \\ &= |\varepsilon_{in} \exp(-j2\pi f_0 t) + \varepsilon_{rbs} \exp\{-j[2\pi(f_0 + \Delta f)t + \varphi_{RB}(t)]\}|^2 \\ &= \varepsilon^2{}_{in} + \varepsilon^2{}_{rbs} + 2\varepsilon_{in}\varepsilon_{rbs} \cos(2\pi\Delta f t + \varphi_{RB}(t)) \end{aligned} \tag{3}$$

$$\begin{aligned} I_{RBSS1}(t) &= |E_{s1}(t) + E_{RBS1}(t)|^2 \\ &= |\varepsilon_\tau \exp[-j(2\pi f_0 t + \varphi(t))] + \varepsilon_{rbs} \exp\{-j[2\pi(f_0 + \Delta f)t + \varphi_{RB}(t)]\}|^2 \\ &= \varepsilon_\tau{}^2 + \varepsilon^2{}_{rbs} + 2\varepsilon_\tau\varepsilon_{rbs} \cos(2\pi\Delta f t + \varphi(t) - \varphi_{RB}(t)) \end{aligned} \tag{4}$$

Optics EXPRESS

Considering the frequency shift of the CW beam, I_{S2} and noise terms I_{RBS2}, I_{RBSS2} can be expressed as:

$$\begin{aligned} I_{S2}(t) &= |E_{r2}(t) + E_{s2}(t)|^2 \\ &= |\varepsilon_{in}\exp\{-j[2\pi(f_0+\Delta f)t]\} + \varepsilon_\tau \exp\{-j[2\pi(f_0+\Delta f)t+\varphi(t)]\}|^2 \\ &= \varepsilon^2{}_{in} + \varepsilon^2{}_\tau + 2\varepsilon_{in}\varepsilon_\tau\cos\varphi(t) \end{aligned} \tag{5}$$

$$\begin{aligned} I_{RBS2}(t) &= |E_{r2}(t) + E_{RBS2}(t)|^2 \\ &= |\varepsilon_{in}\exp\{-j[2\pi(\omega_0+\Delta\omega)t]\} + \varepsilon_{rbs}\exp[-j(2\pi f_0 t+\varphi_{RB}(t))]|^2 \\ &= \varepsilon_{in}{}^2 + \varepsilon^2{}_{rbs} + 2\varepsilon_{in}\varepsilon_{rbs}\cos(2\pi\Delta f t-\varphi_{RB}(t)]\} \end{aligned} \tag{6}$$

$$\begin{aligned} I_{RBSS2}(t) &= |E_{s2}(t) + E_{RBS2}(t)|^2 \\ &= |\varepsilon_\tau\exp\{-j[2\pi(f_0+\Delta f)t)+\varphi(t)] + \varepsilon_{rbs}\exp[-j(2\pi f_0 t+\varphi_{RB}(t))]|^2 \\ &= \varepsilon_\tau{}^2 + \varepsilon^2{}_{rbs} + 2\varepsilon_\tau\varepsilon_{rbs}\cos(2\pi\Delta f t+\varphi(t)-\varphi_{RB}(t)) \end{aligned} \tag{7}$$

Where φ is the phase shift caused by an external disturbance, φ_{RBS} is the vibration-induced phase shift carried by RBS. ε_{in}, ε_τ and ε_{rbs} are the field amplitudes of reference light, sensing light and RBS respectively. They can be expressed by the following [21]:

$$\varepsilon_{in} = \frac{\sqrt{I_0}}{2} \tag{8}$$

$$\varepsilon_\tau = \frac{\sqrt{I_0\exp(-\alpha L)}}{2} \tag{9}$$

$$\varepsilon_{rbs} = \int_0^L \sqrt{\frac{I_0 S\alpha_s(1-\exp(-2\alpha l))}{8\alpha}}dl \tag{10}$$

Where I_0 is the output intensity of the laser, α_s is the attenuation coefficient due to RBS, α is the total attenuation coefficient of the sensing fiber, L is the length of the sensing fiber, S is the fiber recapture factor. Then the intensity of I_{S1} and noise components I_{RBS1} and I_{RBSS1} are analyzed. To simplify the expression, we consider only the amplitude variations of the AC component. For AC coupled BPDs, the DC component is discarded in Eqs. (2–4), and the amplitudes of the AC components A_s, A_{n1} and A_{n2} can be express as:

$$A_s = 2\varepsilon_{in}\varepsilon_\tau = \frac{I_0\exp(-\alpha L/2)}{2} \tag{11}$$

$$A_{n1} = 2\varepsilon_{in}\varepsilon_{rbs} = \frac{I_0}{2}\int_0^L \sqrt{\frac{S\alpha_s(1-\exp(-2\alpha l))}{2\alpha}}dl \tag{12}$$

$$A_{n2} = 2\varepsilon_\tau\varepsilon_{rbs} = I_0\int_0^L \sqrt{\frac{S\alpha_s\exp(-\alpha L)(1-\exp(-2\alpha l))}{8\alpha}}dl \tag{13}$$

Equations (11–13) show that for a single photodetector, as the sensing range increases, A_S decreases exponentially and the noise term $A_n = A_{n1} + A_{n2}$ increases slowly. The simulation results of A_s, A_n and signal-to-noise ratio (SNR) as a function of distance along the fiber are plotted in Fig. 2. It can be seen that if the AC component frequency of I_{S1} and $I_{NB1} = I_{RBS1} + I_{RBSS1}$ are the same, the SNR will gradually decrease with distance, and this common-mode noise is difficult to filter out.

The interference pattern occurring in Hybrid 1 and Hybrid 2 are shown in Fig. 1(b) and (c). Due to the same frequency of sensing and reference light, it can be regarded as a homodyne

Optics EXPRESS

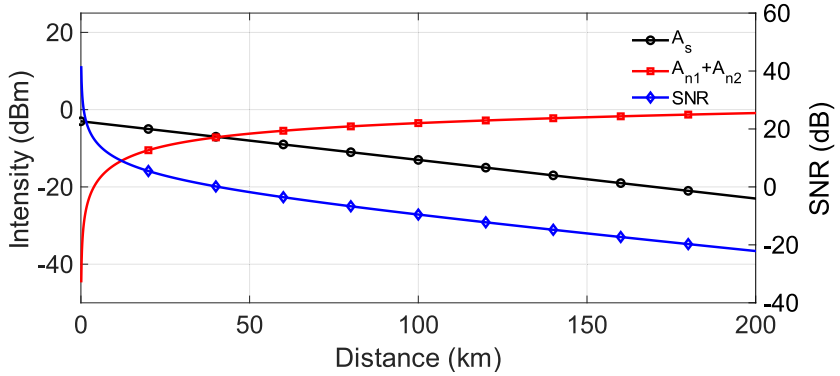

Fig. 2. Simulation results of A_s, A_n and SNR as a function of distance

interference. The interference intensity signal and its phase information carried is located near the baseband. There is a frequency difference between RBS and the reference light, as such it is considered a heterodyne interference. The interference result contains a carrier-band with a frequency of Δf, and the phase information carried by RBS is located near the carrier-band. The common-mode noise can be removed to the considerable frequency difference via the AOM shifting the frequency of the CW beam. The interference intensity signal is converted into an electrical signal by the BPD and sampled by the USB oscilloscope. Lastly, the RBS noise can be filtered out by using a low-pass filter.

The key step in positioning vibrations along the sensing fiber in FTDVS is to calculate the time delay between two copies of vibration-modulated phases signals received by the BPDs at the two detection ends. To simplify the phase-based mathematical model, the effects of optical attenuation and DC components are neglected. Now, Eq. (2) and Eq. (5) can be simplified to:

$$\begin{cases} I_{S1}(t) = \cos[\varphi(t - t_1)]\} \\ I_{S2}(t) = \cos[\varphi(t - t_2)]\} \end{cases} \tag{14}$$

Where $t_1 = (L - Z) \times n/c$ and $t_2 = Z \times n/c$ are the arrival times of the probe light after departing from the vibration position Z respectively. The phase information $\varphi_1(t) = \varphi(t - t_1)$ and $\varphi_2(t) = \varphi(t - t_2)$ can be extracted using a standard coherent IQ detection method widely used in optical communications, using the sine and cosine outputs to retrieve the phase signal. Assuming Δt is the time delay between the vibration-modulated phase signals at the detection ends of two Hybrid, Δt can be expressed as:

$$\Delta t = t_1 - t_2 = \frac{(L - Z) \times n}{c} - \frac{Z \times n}{c} = \frac{n(L - 2Z)}{c} \tag{15}$$

Then the vibration position Z can be obtained by the following equation:

$$Z = \frac{L - \Delta t \times c}{2n} \tag{16}$$

It can be seen from the above equation that the vibration position is only related to the time delay difference Δt. Where Δt can be determined by applying the cross-correlation algorithm between the pair of counter-propagating phase modulation signals: $\varphi_1(t)$ and $\varphi_2(t)$.

Optics EXPRESS

3. Experiment results

3.1. In-lab demonstration

In order to demonstrate that the proposed AFS-FTDVS system can correctly separate the RBS and forward transmitted signals, a comparative experiment was set up. Firstly, the AOM was removed between OC1 and OC3 in Fig. 1(a), so the optical output from Cir1 and Cir2 share the same optical frequency. Then a SMF link with length of 160 km is connected to Cir1 and Cir2. A piezoelectric transducer (PZT) is driven by a 500 Hz sinusoid signal, placed near Cir1. The distribution of I_S and I_{NB} is surveyed by calculating the power spectral density (PSD) of interference intensity signal received by BPD1 (Thorlabs, PDB470C) with 400 MHz bandwidth. The results are shown in Fig. 3(a). The periodic expansion and contraction produced by the PZT imparts a phase modulation on light propagating through the optical fiber, which changes the frequency of the interference intensity signal. In the frequency domain, it can be viewed as the broadening of the center frequency. As can be seen from the figure, I_S and I_{NB} superimpose in the frequency domain due to their equal center frequencies. Figure 3(c) shows the demodulated phase information from Hybrid1 ($\varphi_1(t)$) and Hybrid2 ($\varphi_2(t)$) without an AOM. The phase demodulation method uses the two components generated by each 90° optical hybrid for IQ demodulation [24]. From Fig. 3(c) it can be found that that $\varphi_1(t)$ exhibits low SNR and $\varphi_2(t)$ cannot recover the sinusoidal signal. The control group inserted the AOM between OC1 and OC3 in the CW beam path. The PSD results with the inclusion of the AOM are shown in Fig. 3(b). Due to the frequency shift of CW beam by AOM, I_S and I_{NB} are separated in the frequency domain and the amplitude difference is 14.23 dB. The time domain signals of the 4 channels are demodulated after passing through the low-pass filter to remove the I_{NB} component. Both $\varphi_1(t)$ and $\varphi_2(t)$ can restore the sinusoidal signal and possess high SNR. The demodulation results shown in Fig. 3(d).

In order to verify the vibration detection and positioning ability of the AFS-FTDVS system for long-distance applications, different types of vibration signals are tested. The sensing fiber length is set to approximately 202 km. As mentioned above, I_{NB} has been shifted to the 200 MHz band and can be filtered out using a low-pass filter. In practice, using BPD with bandwidth below 200 MHz and a lower sampling rate can reduce the necessity of using low-pass filter, which can save computational time. BPDs with bandwidth of 100 Hz-75 MHz (Thorlabs, PDB425C) is used in subsequent experiments. The sampling interval *Tin* of the oscilloscope is set to 1,008 ns, and the sampling rate *Fs* is 992 kHz (1/*Tin*). Firstly, a narrowband sinusoidal signal of 400 Hz drives a PZT to produce vibrations. The PZT is coiled with 60 m of optical fiber and the center position is placed at 202,257 m. To avoid interference from low-frequency disturbances, a 20 Hz high-pass filter is applied to the phase signal prior to cross-correlation positioning. Fig. 4(a) shows the demodulated phase signal. It can be seen that both $\varphi_1(t)$ and $\varphi_2(t)$ can restore the sinusoidal signal and exhibit high SNR. The time delay between the two sets of phase signals is 989.85 us, the corresponding vibration position is 202,134 m and the position error is 123 m (can be zeroed through calibration).

In order to further simulate real vibrations, two types of broadband vibrations were artificially generated. The first scenario was to stretch the optical fiber at a frequency of 2 times per second at an actual position of 202,257 m. The demodulated phase signal is shown in Fig. 4(b). The time delay between the two demodulated phase signals received at the two detection ends is 986.83 us, and the corresponding vibration position is 201,825 m. The positioning error from the true position is 432 m. We use 1 m optical fiber jumper to wind on the steel pipe and connect it at 202,257 m. The second scenario is optical fiber coiled around a steel pipe, and by hitting the pipe, an instantaneous broadband vibration signal is generated. The demodulated phase shown in Fig. 4(c). Compared with the former, the vibration caused by knocking steel pipe has a higher frequency vibration component. The time delay between the two phases demodulated phase signal is 989.85 us, and the corresponding vibration position is 202,134 m. The positioning

Optics EXPRESS

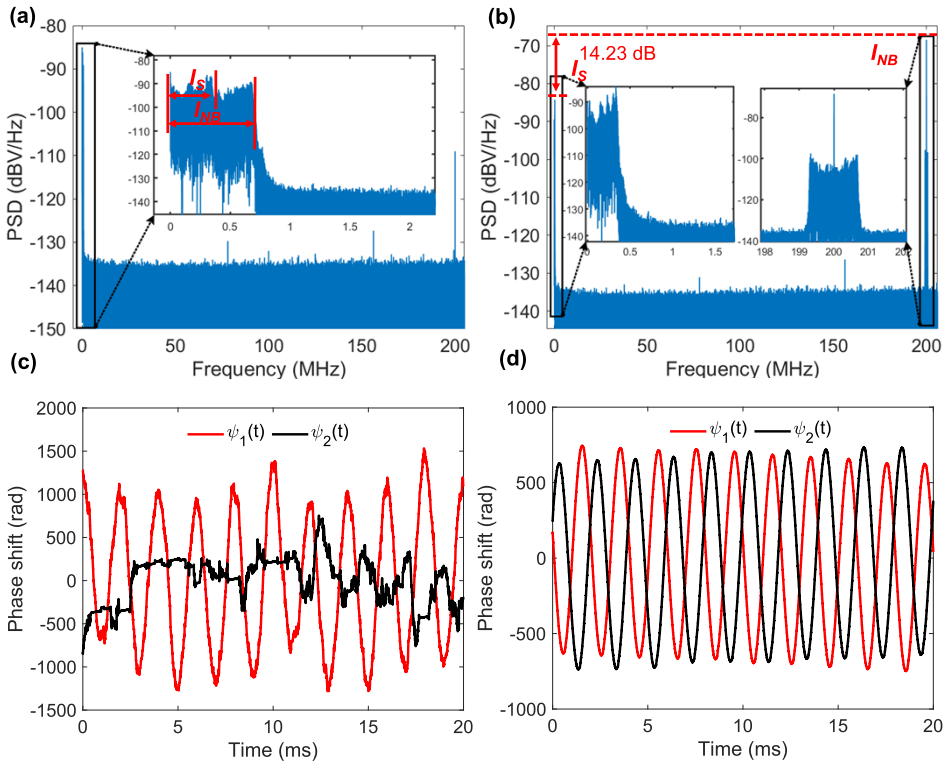

Fig. 3. Interference intensity signal analysis from a 160 km optical fiber link, with a 500 Hz sinusoid vibration signal near Cir1: (a) Power spectral density (PSD) of the signal received by BPD1, without AOM; (b) Power spectral density (PSD) of the signal received by BPD1, with AOM; (c) Demodulated phase signal, without AOM; (d) Demodulated phase signal, with AOM.

error from the true position is 123 m. From the above results, it can be seen that the proposed system structure has superior demodulation and positioning capabilities not only for narrow-band vibration but also wide-band vibration under the sensing length of 202 km.

Through characterizing the phase shift under different fiber strains, their linear relationship and thus the sensitivity was obtained. As shown in Fig. 5(a), by applying 100 Hz sinusoidal signal with different drive voltages (from 0 V to 15 V) to the PZT, the corresponding phase shifts were measured. For each driving voltage, three groups of data were collected to calculate the phase change, and the phase change with the largest difference was 1.93 rad, which occurred at the driving voltage of 6 V. The voltage-strain coefficient of PTZ was measured to be 5.5 με/V. There is a linear relationship between external vibration and phase shift within the tested range of dynamic strain. The signal amplitude and frequency can be extracted through a fast Fourier transform (FFT) on phase signal, which can be seen in Fig. 5(b). The gradient (or sensitivity) of strain vs. phase shift obtained from the linear fitting is 197.22 rad/με.

For the limit of detection (LoD) of the sensing system, two calculation methods are provided. The first method calculates the minimum detectable dynamic strain under frequency-specific conditions, estimated by the following equation:

$$LoD = \frac{mean(\varphi_n)}{sensitivity \times \sqrt{B}} \tag{17}$$

Optics EXPRESS

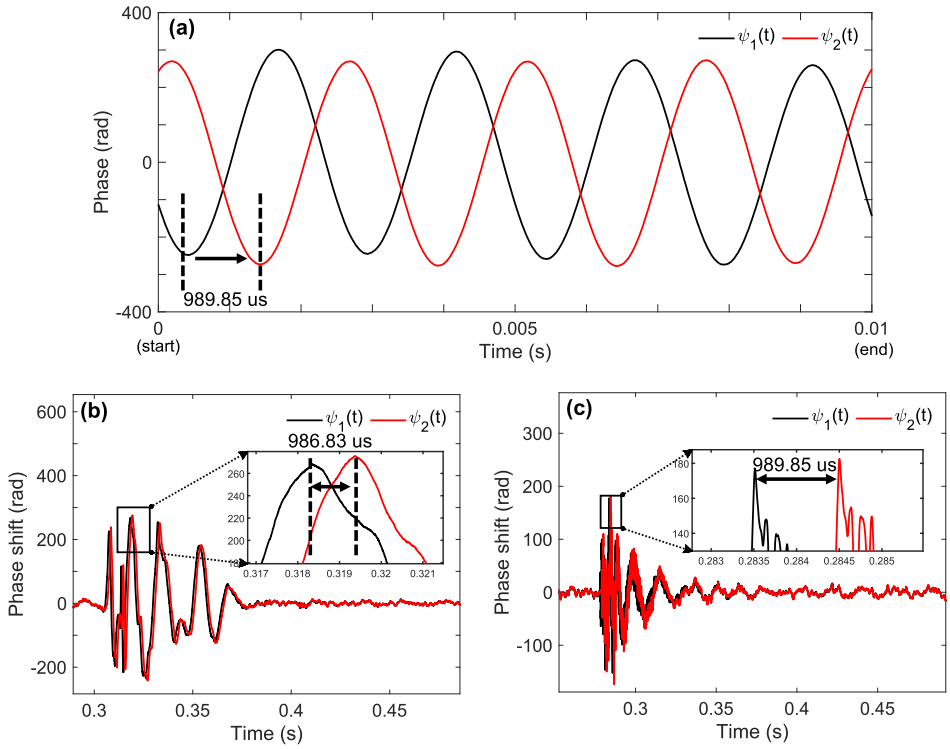

Fig. 4. Phase signals from different perturbations: (a) PZT driven by a 400 Hz sinusoidal signal, the time delay between the two phase signals is 989.85 us, and the corresponding calculated vibration position is 202,134 m (b) stretching the optical fiber by hand, the time delay between the two phase signals is 986.83 us, and the corresponding calculated vibration position is 201,825 m; (c) hitting a steel pipe coiled with 1 m length of optical fiber, the time delay between the two phase signals is 989.85 us, and the corresponding calculated vibration position is 202,134 m.

where φ_n is the noise-equivalent phase amplitude in the absence of external vibration, taken from the highest noise component in the frequency domain (the mean is based on successive readings), and B is the bandwidth of the BPDs. Therefore, based on the mean noise (5.37 rad) and the sensitivity (197.22 rad/με), the LoD is 3.14 pε/Hz$^{1/2}$.

The second method computes the average PSD, and the integrated amplitude of φ_n across the effective bandwidth is calculated to evaluate the LoD. As shown in Fig. 5(c), significant noise amplitude is observed in the low-frequency region (0-20 Hz), while the integrated noise within the effective bandwidth (20 Hz – 496 kHz) averaged at 9.37 rad. Additionally, the LoD was calculated using the effective bandwidth (462 kHz) of the system instead of the BPD bandwidth, yielding 67.46 pε/Hz$^{1/2}$. The discrepancy of the LoD between the two methods can be reduced through ADC sampling rate optimization.

For characterizing the accuracy of vibration positioning (measure of fluctuation, different from positioning error, which takes the mean), successive vibration measurements were carried out, and the experimental results are shown in Fig. 6. In this experiment, 120 datasets of 400 Hz sinusoidal vibration signals was captured. Each measurement duration is 1 s, which ensures sufficient cycles of the signal are present for accurate frequency-domain analysis. For time delay estimation using the cross-correlation algorithm, the spatial resolution (SR) of the positioning

Optics EXPRESS

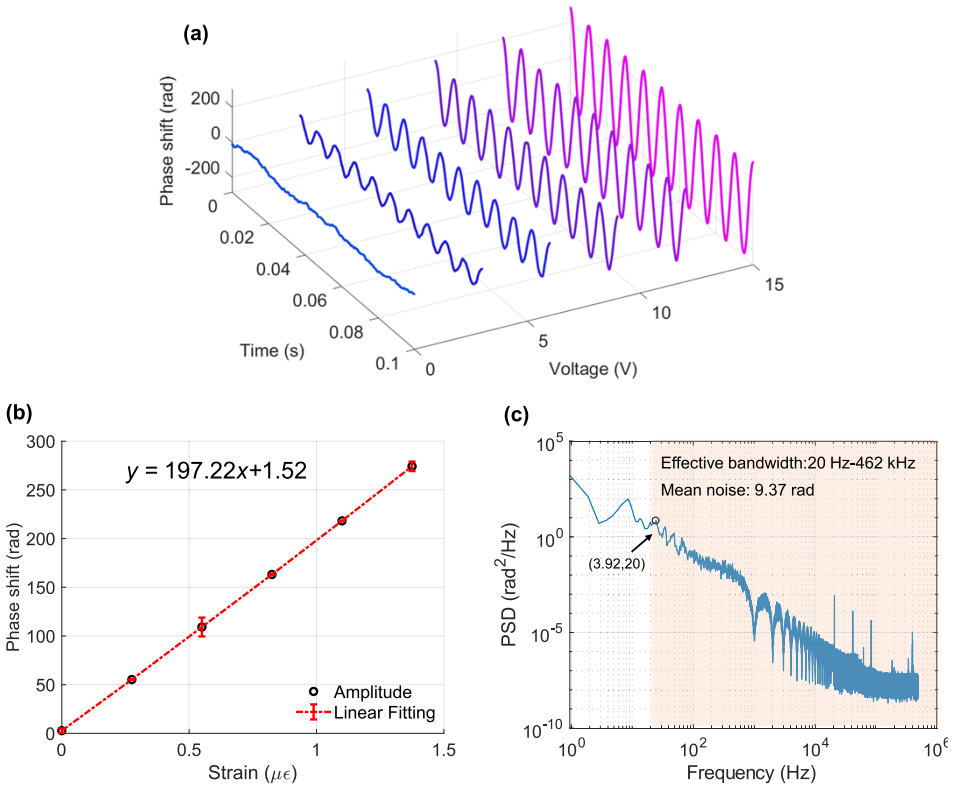

Fig. 5. Strain response and sensitivity: (a) Phase demodulation results of a 100 Hz sine signal with varying amplitudes; (b) Relationship between dynamic strain and phase shift; (c) The mean PSD result of phase noise, the integrated noise across the effective bandwidth is 9.37 rad.

result can be determined by the following equation:

$$SR_{cc} = \frac{Tin \times c}{2n} \tag{18}$$

It can be seen from Fig. 6 that in the 120 repeated positioning experiments, the delay difference between $\varphi_1(t)$ and $\varphi_2(t)$ (original phase) are clustered into 3 values/levels, namely 990.86 us, 989.85 us and 988.85 μs, corresponding to 202,237 m, 202,134 m and 202,031 m, respectively. This is because the SR is larger than the positioning accuracy, thus a certain extend of fluctuation within each quantization level does not result in any change. Interpolating the original phase can improve the positioning accuracy to a certain extent [22]. The original phase was linearly interpolated in the time domain, reducing the original time interval from 1,008 ns to 100.8 ns, and the effective Fs was increased to 9.92 MHz. Correspondingly, the SR improved from 102.86 m to 10.286 m. With the interpolated phase data, the positioning accuracy (STD) was refined from 56.5 m to 46.1 m. This means that the positioning accuracy of the proposed system can reach 0.2% in up to 202 km sensing distance through the use of the cross-correlation algorithm.

In order to test the sensing performance of the system along the sensing fiber with total length of 202,257 m, vibration tests were conducted at five positions. 50 km long optical fiber spools were used to separate each vibration position. The specific positions of the five points on the sensing optical fiber link and the length of each span of optical fiber are shown in Fig. 7(a). Each PZT at the 5 locations served as the vibration source, and was driven with a sinusoidal with

Optics EXPRESS

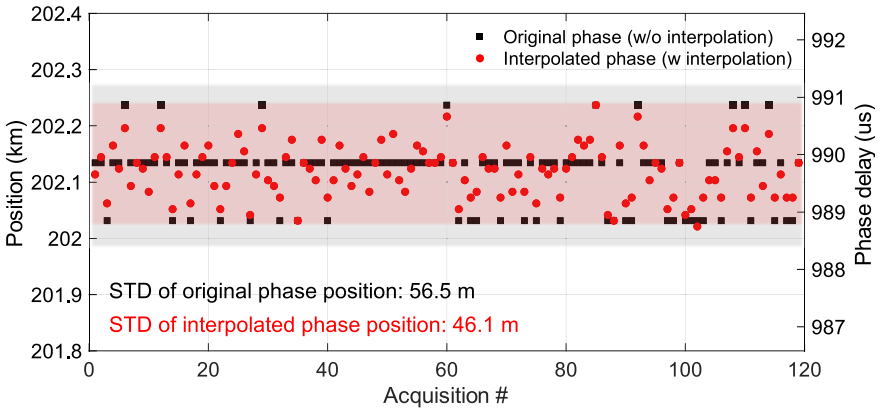

Fig. 6. Vibration positioning repeatability for 202,257 m length fiber link with 400 Hz sinusoidal signal through original (black) phase and linear interpolated phase (red). STD: standard deviation.

an amplitude of 15 V and frequency of 400 Hz. Ten repeated experiments were carried out at each test position. The phase amplitude of the demodulated signal was obtained by FFT. The error bar (+/- 0.23 to +/- 0.57) of amplitude response at each test point is shown in Fig. 7(b). It can be seen from the figure that the amplitude response of each test point has excellent stability. The maximum amplitude deviation point appears at position A, and the difference between the maximum amplitude and the minimum amplitude is 1.12 rad, which corresponding to 5.7 nε. The difference between the maximum amplitude and the minimum amplitude at all test points is only 1.79 rad, which corresponds to 9.1 nε. This is a value that can be ignored in practical applications. Next, 10 repeated measurements were carried out, and the experimental results are shown in Fig. 7(c). The mean value of 10 positioning values is used to represent each test position, and the error distance is the difference between the actual position and the measured position. It can be seen from the figure that both standard deviation (STD) and error distance of the positioning results are relatively small in the middle of the sensing fiber, and larger towards the ends. The largest positioning error of 131 m occurs at position A, and the minimum occurs in at position C, which is only 2 m. This is because a longer optical path difference between the two detection ends results in a different polarization evolution, which leads to a difference in the interference waveform, and ultimately affects the cross-correlation results.

To address the scenario of multiple vibrations, which is very likely to occur in a real measurement environment, the phase-spectrum time delay method [23] for vibration positioning was adopted. This is mathematically similar to performing cross-correlation on the phase signals first, and then Fourier transform is used to obtain the phase spectrum of the signals. The phase difference or time delay for each frequency component between the two detection ends represent the vibration position. Note that this method and other positioning methods for forward-transmission distributed sensing cannot distinguish the vibration influence length on the sensing fiber, nor can they spatially resolve multiple identical-frequency vibration sources. In this case, 230 Hz and 400 Hz vibrations were simultaneously applied at position A and position B, respectively. The demodulated phase signals are shown in Fig. 8(a). From the amplitude spectrum presented in Fig. 8(b), it is evident that the 230 Hz and 400 Hz phase signals are clearly detectable, with a high signal-to-noise ratio. Using the phase spectrum time delay method, the corresponding time delays for these two frequencies are −988.27 us and −495.6 us, respectively, as shown in Fig. 8(c). These time delays correspond to vibration positions of 284 m and 50,556 m, respectively. This demonstrates that the positioning of multiple vibrations is feasible at the basic level.

Optics EXPRESS

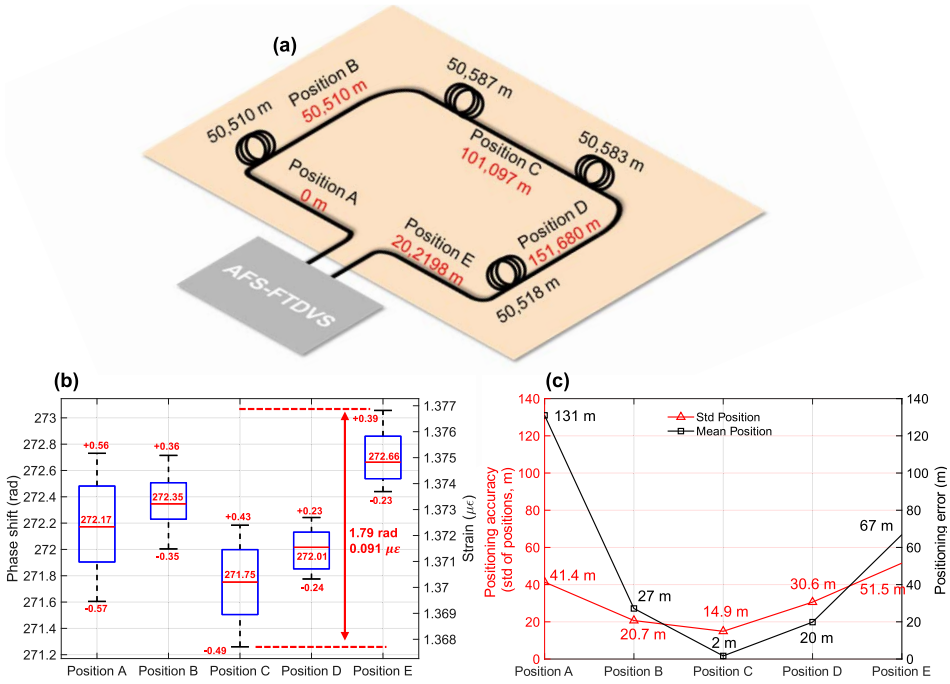

Fig. 7. Vibration measurements at different positions: (a) Fiber link labelled with the position of vibration points on the sensing fiber (red) and the length of each fiber span (black); (b) The deviations of phase amplitude at each vibration point; (c) The positioning characterization for each vibration point.

In order to explore the upper limit of sensing distance of the proposed system, a fiber link with a total length of 272,847 m was established, and PZT was placed at a position of 151,680 m. The optical fiber used in the experiments is the most common single-mode fiber (G.652.D) with an attenuation of 0.18 dB/km at the operating wavelength. The output power of the laser source is 16 dBm. After the attenuation of the various components at the transmitter end, the optical power output from Cir 1 and Cir 2 to the sensing fiber is 4.23 dBm and 7.61 dBm (insertion loss of AOM is ~3 dB), respectively. With a 400 Hz sinusoidal signal applied to the PZT to create vibrations, the demodulated phase signal is shown in Fig. 9(a). It can be seen from that after a transmission distance of 272,847 m, the phase signal still retains a relatively high SNR. Twenty datasets of the vibration signal were captured, and their positioning results are shown in Fig. 9(b). The STD of 20 repeated positioning measurements is 35.6 m (positioning accuracy), and the mean position result is 151,584, which is only 96 m (positioning error) different from the actual positioning. To the best of our knowledge, this is the longest reported sensing distance for FTDVS without optical amplification. Note that the sensing distance can be further enhanced through the removal of fiber connectors (10×0.5 dB = 5 dB loss), switch to avalanche photodiodes and ultra-low-loss optical fiber, as well as optical amplification.

3.2. *Tensile response of submarine optical cables*

In order to simulate the low signal frequencies and large strains experienced by telecom submarine cables in the ocean, a microcomputer-controlled horizontal stretching machine was employed to stretch a section of submarine optical cable (layered stranded optical cable) and the optical response was measured. The experiment design of submarine cable tensile test is shown in Fig. 10(a). A section of submarine cable was placed in the tensile machine. Multiple single-mode

Optics EXPRESS

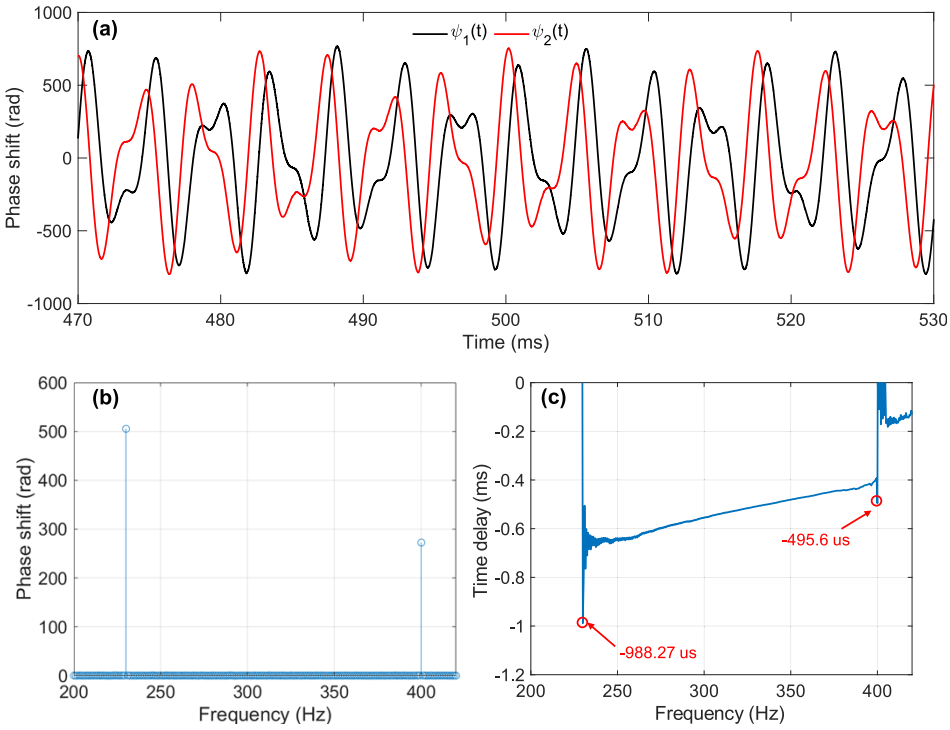

Fig. 8. Multi-point vibrations measurements: (a) Phase signal of two vibration points; (b) Phase amplitude spectrum from FFT; (c) Phase time-delay spectrum.

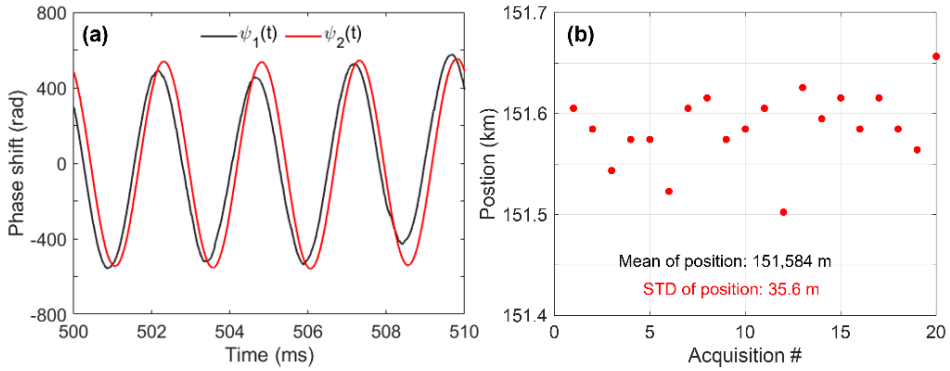

Fig. 9. Positioning results of a vibration situated at 151,680 m along a 272,847 m fiber link: (a) Phase demodulation results of a 400 Hz sinusoidal vibration signal; (b) Vibration positioning repeatability test.

optical fibers embedded in the submarine cable are connected end-to-end to form a link with a fiber length of 1.26 km. The stretching machine is placed in the middle of the two optical fiber spans, and the fiber lengths of the two optical fiber spans are 97.65 km and 85.4 km respectively. The layout of the stretching machine and test site are shown in Fig. 10(b) and Fig. 10(c), respectively. One end of the stretching machine perturbs the submarine cable with a sinusoidal motion at a frequency of 0.15 Hz. Correspondingly, the force loaded onto the submarine cable ranged from 114 kN to 190 kN.

Optics EXPRESS

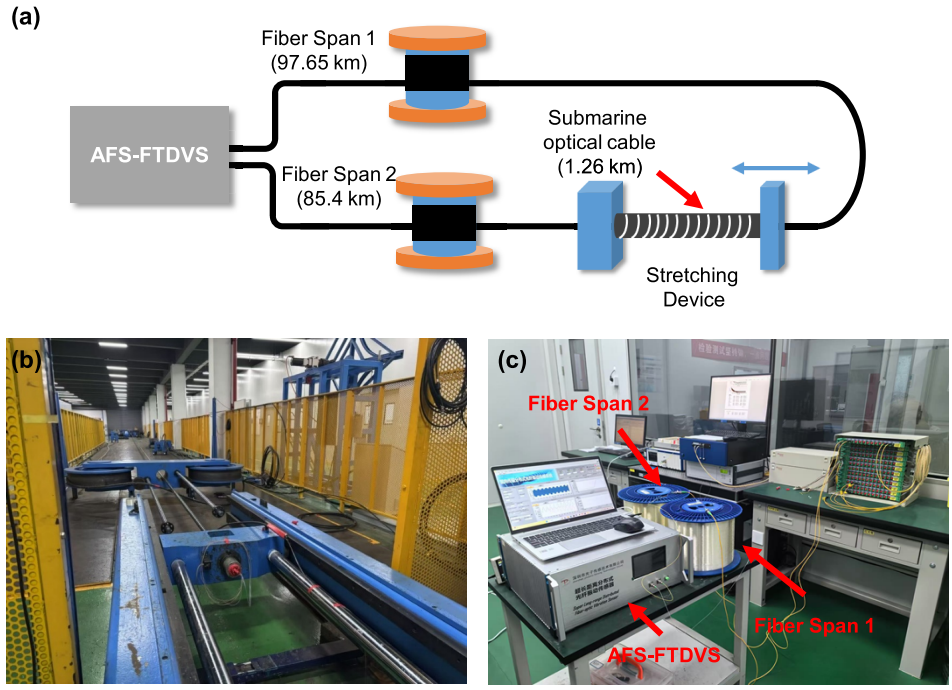

Fig. 10. Tensile testing of submarine cable: (a) Schematic of experiment; (b) Microcomputer-controlled axial tensile machine; (c) Submarine optical cable instrumentation room.

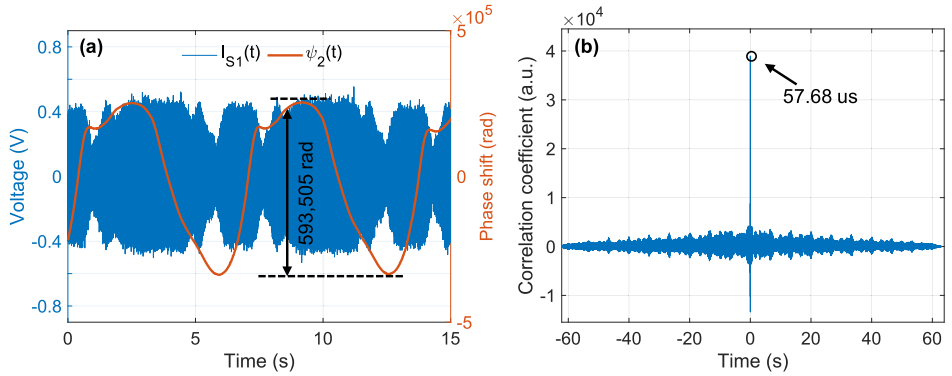

Fig. 11. Phase response of submarine cable under tensile testing: (a) Demodulated phase signal $\varphi_1(t)$ and interference (blue) intensity I_{S1} received by the BPD; (b) Cross-correlation results between I_{S1} and I_{S2}.

The tensile test results of the submarine cable are shown in Fig. 10. The sampling rate of the sensing system is 317.25 kHz. The phase modulation signal caused by cable stretching is plotted in Fig. 11(a) which reveals a waveform resembling a sine wave. The frequency of the phase signal is 0.15 Hz, which is the same as the tensile frequency of the stretching machine. Even though this frequency falls outside the system's effective bandwidth, due to significant fiber elongation, the resulting strain-induced phase signal is still visible. The amplitude of the phase signal is 593,505 rad and the corresponding fiber strain is 1504.7 με according to the pre-determined sensitivity. Since the frequency of the demodulation phase signal is very low and the bandwidth is narrow, the effectiveness of the phase-based cross-correlation algorithm is

Optics EXPRESS

poor. Hence, the interference light intensity signal received by BPD 1 and BPD 3 is used for cross-correlation instead. The sampling rate is increased by 10 times through linear interpolation to increase the SR. The results of cross-correlation are shown in Fig. 11(c). The maximum peak position of the cross-correlation spectrum appears at 57.68 μs. By introducing the delay time into the Eq. (16), it can be calculated that the center position of the submarine cable perturbation is 98,041 km, which exhibits a difference of 391 m from the actual position. This result can be considered adequate for long sensing lengths up to 180 km.

4. Discussion

The proposed system can be implemented in an alternate way: the output E_{r1} from OC2 in Fig. 1(a) connects to Hybrid2 for beat-frequency interference with E_{s2}, while the output E_{r2} from OC3 connects to Hybrid2 for beat-frequency interference with E_{s1}. This configuration shifts the forward-propagating sensing signal to carrier-band with a frequency of Δf, then extract I_S through a high-pass filter. The benefit of this setup is the avoidance of baseband noise, thereby further enhancing the system's SNR (analogous to the function of phase generated carrier demodulation). However, this modification necessitates a higher sampling rate for signal acquisition (>tens of MHz) and imposes a greater computational load. This also creates frequency band redundancy for low-frequency signal acquisition. Alternatively, employing an AOM with 80 MHz operating frequency for shifting is a more economical setup. This allows for the use of a lower-frequency drive signal, a BPD of narrower bandwidth, and a lower sampling rate (BPD bandwidth must be less than the shift frequency). However, when measuring high-frequency or large-amplitude vibrations, the spectral broadening of the interference intensity signal becomes significant. This can easily lead to spectral aliasing between the I_S and the I_{RBS}. In such cases, an AOM with a higher operating frequency offers a broader frequency response range.

5. Conclusion

Backscatter noise is detrimental to long-distance distributed fiber-optic vibration sensors that operate with forward transmission of probe light. The AFS-FTDVS method is proposed to separate Rayleigh backscatter (RBS) noise from forward transmitted signals in the frequency domain through an elegant frequency-shift approach. The AFS-FTDVS structure provides reliable positioning for both single frequency and broadband vibrations. At a maximum sensing distance of 272 km (without any optical amplification), the positioning accuracy can be as good as 35.6 m. To the best of our knowledge, this is the longest reported sensing distance for FTDVS without optical amplification. The experiment results conducted at different positions on the sensing link prove that the sensing performance of the system exhibits fair consistency, with the maximum difference in vibration amplitude being 9.1 nε. With a sampling rate of 992 kHz, the system's frequency response ranges from 20 Hz to 496 kHz. After phase demodulation and interpolation, the effective rate is 9.92 MHz and the standard deviation in positioning is 46.1 m. The LoD and sensitivity of the system are 3.14 pε/Hz$^{1/2}$ and 197.22 rad/με respectively in 202 km sensing range. The phase-spectrum time delay algorithm facilitates multi-point positioning. In order to simulate the low frequency and large dynamic strain experienced by submarine cables in the ocean, a microcomputer-controlled axial tensile machine was employed to stretch a section of submarine cable, while the AFS-FTDVS system carried out signal demodulation and positioning.

Funding. Ministry of Science and Technology of the People's Republic of China (2022YFE0111400); National Natural Science Foundation of China (U22A2088, 62275172); Shenzhen Science and Technology Program (JCYJ20241202124408012, JCYJ20220818095800001); Shenzhen Science and Technology Program (Shenzhen Key Laboratory of Ultrafast Laser Micro/Nano Manufacturing ZDSYS20220606100405013); Scientific Instrument Developing Program of Shenzhen University (2023YQ027); LingChuang Research Project of China National Nuclear Corporation.

Disclosures. The authors declare no conflicts of interest.

Optics EXPRESS

Data availability. Data underlying the results presented in this paper are not publicly available at this time but may be obtained from the authors upon reasonable request.

References

1. M. Nie, J. Xu, J. Yu, *et al.*, "Ultra long single span distributed sensing distance over 200 km based on the phase-sensitive OTDR with bidirectional high-order Raman amplification," in *2021 19th International Conference on Optical Communications and Networks (ICOCN)*, (IEEE, 2021), 01–3.
2. Z. Wang, J. Zeng, J. Li, *et al.*, "175 km phase-sensitive OTDR with hybrid distributed amplification," in *23rd international conference on optical fibre sensors*, (SPIE, 2014), 1562–1565.
3. J. Li, Z. Wang, L. Zhang, *et al.*, "124 km phase-sensitive OTDR with Brillouin amplification," *OFS2014 23rd International Conference on Optical Fiber Sensors* (SPIE, 2014), Vol. 9157.
4. J. Li, Y. Wang, P. Wang, *et al.*, "Detection range enhancement for Φ-OTDR using semantic image segmentation," J. Lightwave Technol. **40**(14), 4886–4895 (2022).
5. H. Wijaya, P. Rajeev, E. Gad, *et al.*, "Distributed optical fibre sensor for infrastructure monitoring: Field applications," Opt. Fiber Technol. **64**, 102577 (2021).
6. Y.-H. Lin, B.-H. Zheng, L. Wang, *et al.*, "Cascaded fiber-optic interferometers for multi-perimeter-zone intrusion detection with a single fiber used for each defended zone," IEEE Sens. J. **21**(9), 10685–10694 (2021).
7. K. Bremer, F. Weigand, Y. Zheng, *et al.*, "Structural health monitoring using textile reinforcement structures with integrated optical fiber sensors," Sensors **17**(2), 345 (2017).
8. W. Png, H. S. Lin, C. H. Pua, *et al.*, "Feasibility use of in-line Mach–Zehnder interferometer optical fibre sensor in lightweight foamed concrete structural beam on curvature sensing and crack monitoring," Struct. Health Monitoring **17**(5), 1277–1288 (2018).
9. H. Hsieh, K.-S. Hsu, T.-L. Jong, *et al.*, "Multi-zone fiber-optic intrusion detection system with active unbalanced michelson interferometer used for security of each defended zone," IEEE Sens. J. **20**(3), 1607–1618 (2020).
10. S. Shan, L. Wang, J. Zhou, *et al.*, "Leakage detection of oil pipeline using distributed fiber optic sensor," in *International Conference on Smart Materials and Nanotechnology in Engineering*, (SPIE, 2007), 451–456.
11. S. Pi, B. Wang, J. Zhao, *et al.*, "A novel linear Sagnac interferometer in position determination of perturbations," in *Interferometry XVII: Techniques and Analysis*, (SPIE, 2014), 264–269.
12. J. Huang, Y. Chen, H. Peng, *et al.*, "A 150 km distributed fiber-optic disturbance location sensor with no relay based on the dual-Sagnac interferometer employing time delay estimation," Opt. Commun. **479**, 126420 (2021).
13. Q. Chen, Chao Jin, Y. Bao, *et al.*, "A distributed fiber vibration sensor utilizing dispersion induced walk-off effect in a unidirectional Mach-Zehnder interferometer," Opt. Express **22**(3), 2167–2173 (2014).
14. W. Kong, F. Liu, G. Zhu, *et al.*, "Localization enhancement of forward-transmission distributed vibration sensors using phase differentiation endpoint amplification," IEEE Sensors Journal (2024).
15. Y. Yan, F. N. Khan, B. Zhou, *et al.*, "Forward transmission based ultra-long distributed vibration sensing with wide frequency response," J. Lightwave Technol. **39**(7), 2241–2249 (2021).
16. F. Shi, R. Jin, Y. Du, *et al.*, "Ultra-Long-Distance Interferometric DOFS Over 300 km without In-line Repeater," IEEE Photonics Technol. Lett. **37**(5), 289–292 (2025).
17. Z. Zhao, L. Shen, Y. Dang, *et al.*, "Enabling long range distributed vibration sensing using multicore fiber interferometers," Opt. Lett. **46**(15), 3685–3688 (2021).
18. C. Ma, T. Liu, K. Liu, *et al.*, "Long-range distributed fiber vibration sensor using an asymmetric dual Mach–Zehnder interferometers," J. Lightwave Technol. **34**(9), 2235–2239 (2016).
19. X. Rao, Y. Wang, M. Chen, *et al.*, "150 km single-span distributed vibration sensor based on compensated self-interference forward transmission," J. Lightwave Technol. **42**(16), 5736–5742 (2024).
20. K. Liu, P. Ma, J. Jiang, *et al.*, "An S-transform-based positioning method for asymmetric interferometer disturbance sensors," J. Lightwave Technol. **37**(13), 3201–3207 (2019).
21. P. Gysel and R. K. Staubli, "Spectral properties of Rayleigh backscattered light from single-mode fibers caused by a modulated probe signal," J. Lightwave Technol. **8**(12), 1792–1798 (1990).
22. Q. Song, P. Zhou, H. Peng, *et al.*, "Improved localization algorithm for distributed fiber-optic sensor based on merged Michelson-Sagnac interferometer," Opt. Express **28**(5), 7207–7220 (2020).
23. X. Rao, S. Dai, M. Chen, *et al.*, "Multi-point vibration positioning method for long-distance forward transmission distributed vibration sensing," Opt. Express **32**(17), 30775–30786 (2024).
24. Z. Wang, L. Zhang, S. Wang, *et al.*, "Coherent Φ-OTDR based on I/Q demodulation and homodyne detection," Opt. Express **24**(2), 853–858 (2016).